



High photocatalytic activity of Ag/Ag₃PO₄:W heterostructure formed by femtosecond laser irradiation

Aline Barrios Trench¹, Vinícius Teodoro¹, Letícia Guerreiro da Trindade², Thales Rafael Machado¹, Gladys Minguez-Vega³, Eloisa Cordoncillo⁴, Carlos Doñate-Buendía^{3,5}, Juan Andrés⁶, Elson Longo¹⁺

1. Federal University of Sao Carlos, Center for the Development of Functional Materials, São Carlos, Brazil.
2. University of São Paulo, São Carlos Institute of Chemistry, São Carlos, Brazil.
3. University Jaume I, Institut de Noves Tecnologies de la Imatge, Castelló, Spain.
4. University Jaume I, Department of Inorganic and Organic Chemistry, Castelló, Spain.
5. University of Wuppertal, Materials Science and Additive Manufacturing, Wuppertal, Germany.
6. University Jaume I, Department of Analytical and Physical Chemistry, Castelló, Spain.

+Corresponding author: Elson Longo, **Phone:** +55 16 33519588, **Email address:** elson.liec@gmail.com

ARTICLE INFO

Article history:

Received: July 22, 2021

Accepted: September 01, 2021

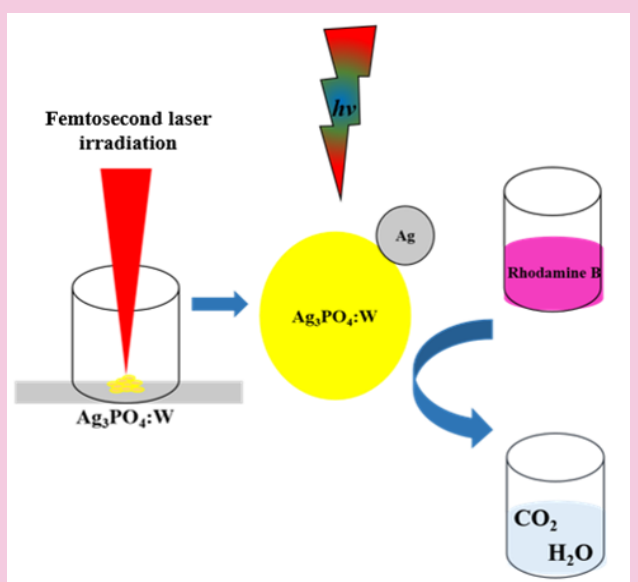
Published: April 11, 2022

Keywords:

1. Ag₃PO₄
2. doping
3. heterostructure
4. photocatalytic property

Section Editors: Elson Longo and Juan Manuel Andrés Bort

ABSTRACT: In this work, the W-doped Ag₃PO₄ was prepared by the chemical coprecipitation method and irradiated with a femtosecond laser (FL). The successful formation of the Ag/Ag₃PO₄:W heterostructure was confirmed by XRD analysis. A higher structural disorder in the [PO₄] clusters was observed for the FL irradiated sample (Ag₃PO₄:W-FL), indicating the formation of Ag metallic from the Ag₃PO₄ structure. The photocatalytic activity of the samples was studied by photodegradation of rhodamine B under visible light irradiation. The formation of Ag nanoparticles on the surface of Ag₃PO₄:W led to a degradation rate constant 3.54 times higher than the nonirradiated sample. This higher photocatalytic activity was related to the surface plasmon resonance effect of the Ag metallic, which acts by capturing photoexcited electrons from the Ag₃PO₄:W, avoiding the recombination of electron-hole pairs, and thus improving the photocatalytic activity.



1. Introduction

Water sources contain various types of contaminants (Sousa *et al.*, 2018), with industrial waste being the contaminants that draw the major attention in environmental pollution, thus requiring a suitable treatment (Karimi-Maleh *et al.*, 2020). Among industrial wastes, organic dyes are the main concern due to their high generated content and toxicity, being of fundamental importance the proper treatment. Rhodamine B (RhB) is an organic dye that can cause damage to humans, leading to skin and eye irritations and respiratory problems (Aljerf, 2018; Dong *et al.*, 2010). Several treatment methods have been studied, such as heterogeneous photocatalysis, which has been considered promising for the treatment of organic dyes because of its green and clean aspects, simplicity and low cost (Zangeneh *et al.*, 2015). Silver phosphate (Ag_3PO_4) has been receiving attention from researchers since its discovery for presenting photocatalytic properties such as the extremely high photooxidative capacity for the evolution of O_2 from water and the decomposition of efficient organic dyes using sunlight (Chen *et al.*, 2015; He *et al.*, 2019; Trench *et al.*, 2018; Zwara *et al.*, 2018). Furthermore, Ag_3PO_4 presents advantages in relation to other well-known photocatalysts, such as TiO_2 , due to its ability to absorb light in the visible region (Fujishima and Honda, 1972). However, Ag_3PO_4 has the disadvantage of photocorrosion and fast recombination of electron-hole pairs, decreasing its stability as a photocatalyst, making its use unfeasible (Chen *et al.*, 2015). Therefore, studies that aim to modify to improve the Ag_3PO_4 photocatalytic activity are of great interest (R. Santos *et al.*, 2020; Shaveisi and Sharafnia, 2020; Shi *et al.*, 2019).

Among the modification methods, the doping process was applied to overcome these disadvantages of Ag_3PO_4 . Our research group has showed a significant improvement of the photocatalytic performance of Mo- and W-doped Ag_3PO_4 (Trench *et al.*, 2018; 2020), while very recently ultra-active Ag_3PO_4 with different W doping rates were successfully synthesized by Trench *et al.*, 2020. Moreover, the deposition of noble nanoparticles, such as Ag, Au, Pt and Pd, onto the surface of Ag_3PO_4 is an important approach to produce a metal semiconductor composite with enhanced photocatalytic performance (Y. Liu *et al.*, 2012; Yan *et al.*, 2014; Z. Liu *et al.*, 2017). This behavior mainly stems from the surface plasmon resonance (SPR) effect of metal nanoparticles, which are related to the collective oscillations of free electrons that can lead to improved visible light absorption, the superior

separation of electron-hole pairs in the composite material, and by the inhibition of photocorrosion mechanisms due to the accumulation of electrons in the Ag nanoparticles instead of Ag_3PO_4 surface (Li *et al.*, 2019).

The decoration of semiconductors with metal nanoparticles is mainly conducted by the adsorption of metal precursors on their surface followed by the chemical reduction in solution (Kochuveedu *et al.*, 2013). Alternatively, the femtosecond laser (FL) irradiation is attracting attention as a cost-effective, fast and clean method for the fabrication of metal-semiconductor heterostructure in which the requirement of organic solvents or chemical reducing agents are minimized (Tan *et al.*, 2013; Vorobyev and Guo, 2013). The short pulses of the laser can induce the nanoparticles formation from distinct bulk targets, as the migration of Ag atoms to the surface of complex oxides followed by their reduction into metallic species (Machado *et al.*, 2018). Our research group reported the formation of Ag nanoparticles on $\alpha\text{-Ag}_2\text{WO}_4$ with superior bactericidal activity (Assis *et al.*, 2018), the laser-induced formation of Ag/Cr particles on AgCrO_4 (Lemos *et al.*, 2019), and the synthesis of Ag-Bi nanoalloys from Ag_2WO_4 and NaBiO_3 targets (Machado *et al.*, 2018). In special, we reported the nucleation and growth of Ag nanoparticles on Ag_3PO_4 surface mediated by FL irradiation (C. Santos *et al.*, 2019). As a step forward, in the present study we demonstrate the formation of $\text{Ag}/\text{Ag}_3\text{PO}_4\text{:W}$ heterostructure by FL irradiation and its superior photocatalytic activity in compare to $\text{Ag}_3\text{PO}_4\text{:W}$, as evidenced by RhB visible light-driven photodegradation process.

2. Materials and methods

2.1 Synthesis of $\text{Ag}_3\text{PO}_4\text{:W}$ and preparation of $\text{Ag}_3\text{PO}_4\text{:W-FL}$ samples

The $\text{Ag}_3\text{PO}_4\text{:W}$ sample was synthesized using the coprecipitation method and doped with 1% mol $\text{Na}_2\text{WO}_4 \cdot 2\text{H}_2\text{O}$, as previously reported by Trench *et al.* (2020).

$\text{Ag}_3\text{PO}_4\text{:W}$ was irradiated with a Ti:sapphire laser (Femtopower Compact Pro, Femto Lasers) using 30 fs full width at half maximum (FWHM) pulses at the central wavelength of 800 nm, and a repetition rate of 1 kHz. A laser beam of 6 mm diameter and mean power of 185 mW was focused onto the surface of $\text{Ag}_3\text{PO}_4\text{:W}$ with a 75 mm lens. To obtain the $\text{Ag}_3\text{PO}_4\text{:W-FL}$ heterostructure, the $\text{Ag}_3\text{PO}_4\text{:W}$ was placed at the bottom of a quartz cuvette attached to a two-dimensional

motion-controlled stage moving in a raster scanning at a constant speed of 0.5 mm s^{-1} in the focus plane perpendicular to the laser beam.

2.2 Characterization techniques

The structural features at long-range of the samples were investigated by X-ray diffraction (XRD) performed in a D/Max-2500PC diffractometer (Rigaku, Japan) using $\text{Cu K}\alpha$ radiation ($\lambda = 1.54056 \text{ \AA}$), at a scan rate of $0.5^\circ \text{ min}^{-1}$. The structural features at short-range of the samples were investigated by micro-Raman scattering spectroscopy measurements performed in a LabRAM iHR550 Horiba Jobin Yvon spectrometer coupled with a charge-coupled device (CCD, Synapse) as a signal detector, and an ion argon laser with 514.5 nm of wavelength (Melles Griot). The optical absorption spectroscopy measurements in the ultraviolet and visible region were performed in the diffuse reflectance mode in a Varian spectrophotometer model Cary 5G (USA) in the range of 250–800 nm. Field emission scanning electron microscopy (FE-SEM) was performed using a FEI microscope (Model Inspect F50) operating at 5 kV.

2.3 Photocatalytic experiments

The photocatalytic activity of $\text{Ag}_3\text{PO}_4\text{:W}$ and $\text{Ag}_3\text{PO}_4\text{:W-FL}$ samples were tested for degradation of RhB (95%, Aldrich) under visible light irradiation. For this experiment, 50 mg of each sample and 50 mL of RhB (10 mg L^{-1}) were used, which were submitted to an ultrasonic bath (Branson, model 1510; frequency 42 kHz) for 5 min and 30 min of constant agitation, in order to reach the adsorption-desorption balance and later exposed to irradiation of six lamps (Philips TL-D, 15 W). Aliquots were taken at 1 min intervals, centrifuged and their degradation monitored by measuring the peak of maximum RhB absorption ($\lambda_{\text{max}} = 554 \text{ nm}$) using an ultraviolet-visible (UV-Vis) spectrophotometer (V-660, JASCO). A test under the same conditions without the presence of catalysts was also carried out.

3. Results and discussion

Figure 1a shows the XRD patterns of $\text{Ag}_3\text{PO}_4\text{:W}$ and $\text{Ag}_3\text{PO}_4\text{:W-FL}$ samples. The diffraction peaks for both samples indicated the cubic phase of Ag_3PO_4 with $P-43n$ space group, according to the Inorganic Crystal Structure Database (ICSD) code 14000 (Masse *et al.*, 1976). No secondary or any dopant related phases were observed for $\text{Ag}_3\text{PO}_4\text{:W}$ sample, indicating the successfully of insertion of W as dopant into the Ag_3PO_4

structure. However, for the sample irradiated with the FL, it was observed the emergence of a peak at approximately 37.8° (2θ), as can be seen in Fig. 1b. The as-mentioned peak is assigned to the (111) diffraction plane of cubic phase of Ag with $Fm-3m$ space group, which is the most intense diffraction peak for this structure, according to the ICSD code 604630 (Jette and Foote, 1935). It is well-known that the FL irradiation in Ag-containing materials, such as Ag_3PO_4 , induces the reduction of Ag^+ cations in the structure for the formation of Ag nanoparticles on the semiconductor surface (Assis *et al.*, 2018; 2019; C. Santos *et al.*, 2019). Herewith, the FL irradiation effectively allowed the formation of $\text{Ag}/\text{Ag}_3\text{PO}_4\text{:W}$ heterostructure in the $\text{Ag}_3\text{PO}_4\text{:W-FL}$ samples.

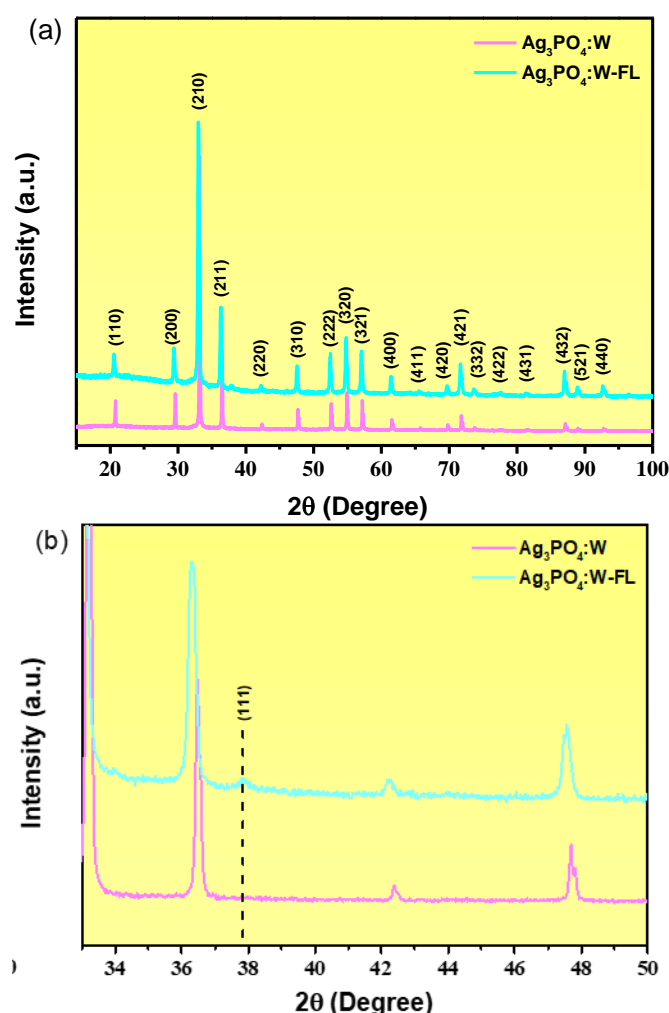


Figure 1. XRD patterns of $\text{Ag}_3\text{PO}_4\text{:W}$ and $\text{Ag}_3\text{PO}_4\text{:W-FL}$ samples in the range of $10\text{--}100^\circ$ (a) and in the range of $33\text{--}50^\circ$ (b).

Figure 2 shows the Raman spectra of $\text{Ag}_3\text{PO}_4\text{:W}$ and $\text{Ag}_3\text{PO}_4\text{:W-FL}$ samples. According to the group theory analysis, the cubic phase of Ag_3PO_4 structure presents

18 Raman active modes ($\Gamma = 2 A_1 + 4 E + 12 T_2$) (Trench *et al.*, 2018; Botelho *et al.*, 2015). The observed Raman bands for the prepared samples are located at approximately 100, 237, 539, 700, 904, and 997 cm^{-1} . All these modes are related to the cubic phase of Ag_3PO_4 and no Raman bands related to any secondary or W dopant phases were observed. The bands located at 100 and 237 cm^{-1} have been assigned to the translational and/or rotational modes with T_2 symmetry of $[\text{PO}_4]$ clusters. The band located at 539 cm^{-1} is assigned to the bending mode with T_2 symmetry of $[\text{PO}_4]$ clusters. The band located at 700 cm^{-1} is attributed to the symmetric stretching mode of the $[\text{PO}_4]$ clusters. The most intense band located at 904 cm^{-1} is related to the symmetric stretching (A_1) mode, whereas the band located at 997 cm^{-1} is related to the asymmetric stretching mode (T_2) mode of $[\text{PO}_4]$ clusters.

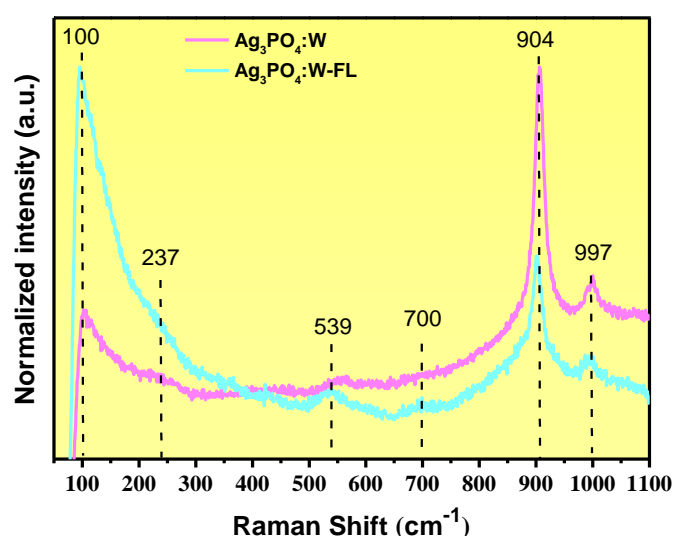


Figure 2. Raman spectra of $\text{Ag}_3\text{PO}_4:\text{W}$ and $\text{Ag}_3\text{PO}_4:\text{W-FL}$ samples.

It can be observed that the $\text{Ag}_3\text{PO}_4:\text{W-FL}$ sample presented a remarkable decrease of the relative intensity of the band at 904 cm^{-1} compared to the $\text{Ag}_3\text{PO}_4:\text{W}$ sample. As observed in XRD results, the FL irradiation in $\text{Ag}_3\text{PO}_4:\text{W}$ sample induced the formation of metallic Ag that arises from the reduction of Ag^+ cations in the Ag_3PO_4 structure. This process generates Ag vacancies in the structure, which induce a local structural rearrangement of the adjacent $[\text{PO}_4]$ clusters. This rearrangement causes variations in the coordination parameters of the clusters, *i.e.*, bond angles and lengths, thus increasing the structural disorder in the $[\text{PO}_4]$ clusters. The structural disorder in the clusters leads to a break of local symmetry that decreases the freedom degree of vibrational modes the $[\text{PO}_4]$ clusters, hence decreasing the intensity of Raman scattering.

UV-Vis diffuse reflectance measurements were employed to determine the optical band gap energies of the prepared samples. Considering that the absorption spectrum of the Ag_3PO_4 is governed by indirect electronic transitions (Botelho *et al.*, 2016), Fig. 3a and b show the Tauc plot (Wood and Tauc, 1972) for the $\text{Ag}_3\text{PO}_4:\text{W}$ and $\text{Ag}_3\text{PO}_4:\text{W-FL}$ samples, respectively. It can be observed a slight decrease in the band gap energy for the $\text{Ag}_3\text{PO}_4:\text{W-FL}$ compared to the $\text{Ag}_3\text{PO}_4:\text{W}$ sample, being the values of 2.53 and 2.43 eV, respectively. As previous mentioned in Raman analysis, the FL irradiation in the $\text{Ag}_3\text{PO}_4:\text{W}$ sample induced structural disorder in the $[\text{PO}_4]$ clusters due to the formation of Ag vacancies in the Ag_3PO_4 structure. These structural distortions induce the formation of intermediate energy levels within the band gap, which can act as electron traps, thus decreasing the band gap energy of the FL irradiated sample.

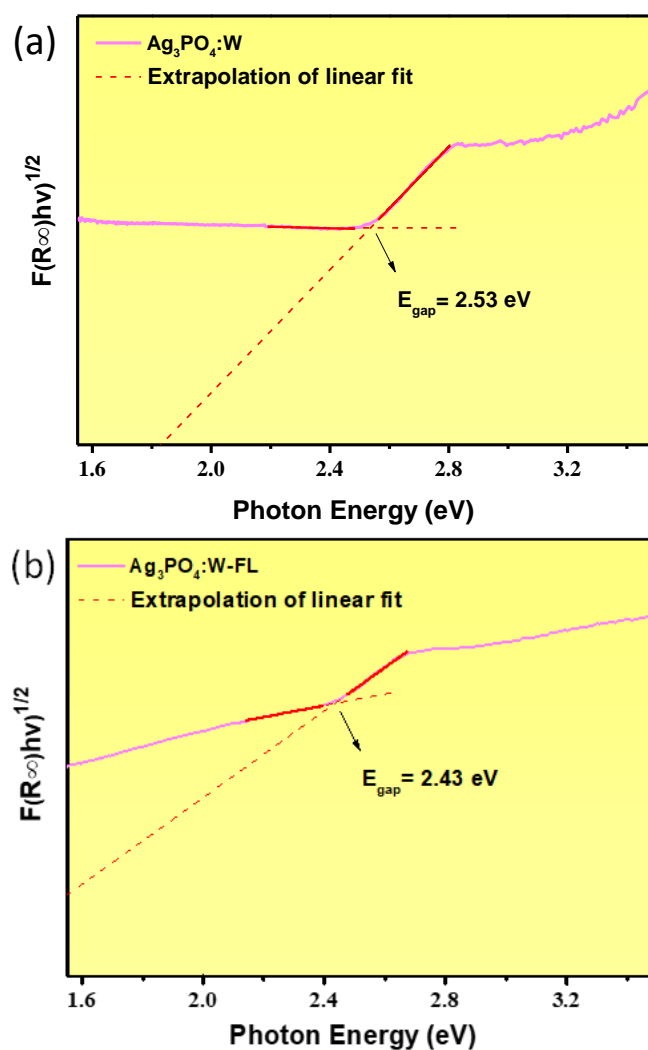


Figure 3. Tauc plot for the $\text{Ag}_3\text{PO}_4:\text{W}$ (a) and $\text{Ag}_3\text{PO}_4:\text{W-FL}$ (b) samples.

The morphological aspects of the $\text{Ag}_3\text{PO}_4\text{:W}$ and $\text{Ag}_3\text{PO}_4\text{:W-FL}$ samples were investigated by FE-SEM analysis. Figure 4a and b shows the FE-SEM images of the $\text{Ag}_3\text{PO}_4\text{:W}$ and $\text{Ag}_3\text{PO}_4\text{:W-FL}$ samples, respectively, with their corresponding insets with magnified regions of the images. For the $\text{Ag}_3\text{PO}_4\text{:W}$ sample, it can be observed nano- and microparticles with quasi-spherical shape. These morphologies are similar to those previously reported (Trench *et al.*, 2018; 2020). However, the FE-SEM image of the $\text{Ag}_3\text{PO}_4\text{:W-FL}$ sample presents smaller and agglomerated particles compared to the $\text{Ag}_3\text{PO}_4\text{:W}$ sample. These aspects arise from the high local energy of the pulsed FL in the sample, thus inducing the fragmentation and coalescence of the particles. Moreover, according to reported works (Assis *et al.*, 2018; C. Santos *et al.*, 2019) and the XRD results, the presence of nanoparticles on the surface of larger particles can be assigned to the Ag metallic nanoparticles.

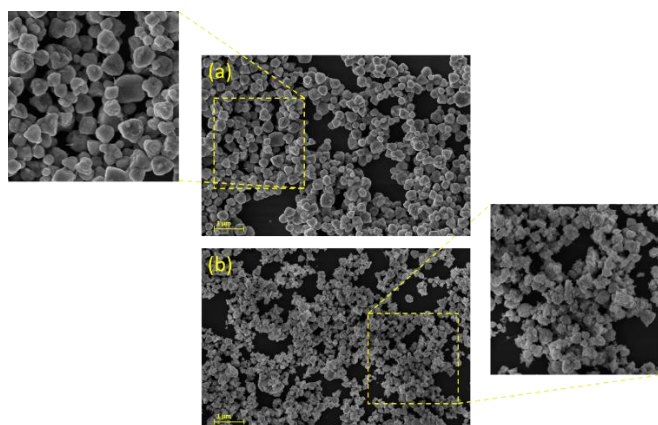


Figure 4. FE-SEM images of $\text{Ag}_3\text{PO}_4\text{:W}$ (a) and $\text{Ag}_3\text{PO}_4\text{:W-FL}$ (b) samples.

The photocatalytic activity of the $\text{Ag}_3\text{PO}_4\text{:W}$ and $\text{Ag}_3\text{PO}_4\text{:W-FL}$ samples were investigated by the degradation of RhB under visible light irradiation. Figure 5a shows the degradation efficiency of both prepared samples and the control experiment without photocatalyst. As can be seen, no significant degradation was observed in the absence of photocatalyst. As previously reported, the $\text{Ag}_3\text{PO}_4\text{:W}$ sample presents a highly photocatalytic activity for RhB degradation under visible light irradiation, allowing approximately 82.5% of RhB degradation in only 3 min of reaction (Trench *et al.*, 2020). However, it was observed a remarkable improvement of the photocatalytic activity of the FL irradiated sample, allowing 100% of RhB degradation in 3 min of reaction. To further compare, the $\text{Ag}_3\text{PO}_4\text{:W}$ and $\text{Ag}_3\text{PO}_4\text{:W-FL}$ samples promoted 60.5% and 97.2% of RhB in only 2

min of reaction. Figure 5b shows the Langmuir-Hinshelwood plot for the pseudo first-order kinetics model (B. Liu *et al.*, 2014) for both prepared samples and the control experiment. It was observed that the $\text{Ag}_3\text{PO}_4\text{:W-FL}$ sample presented a rate constant (k) 3.54 times higher than the $\text{Ag}_3\text{PO}_4\text{:W}$ sample.

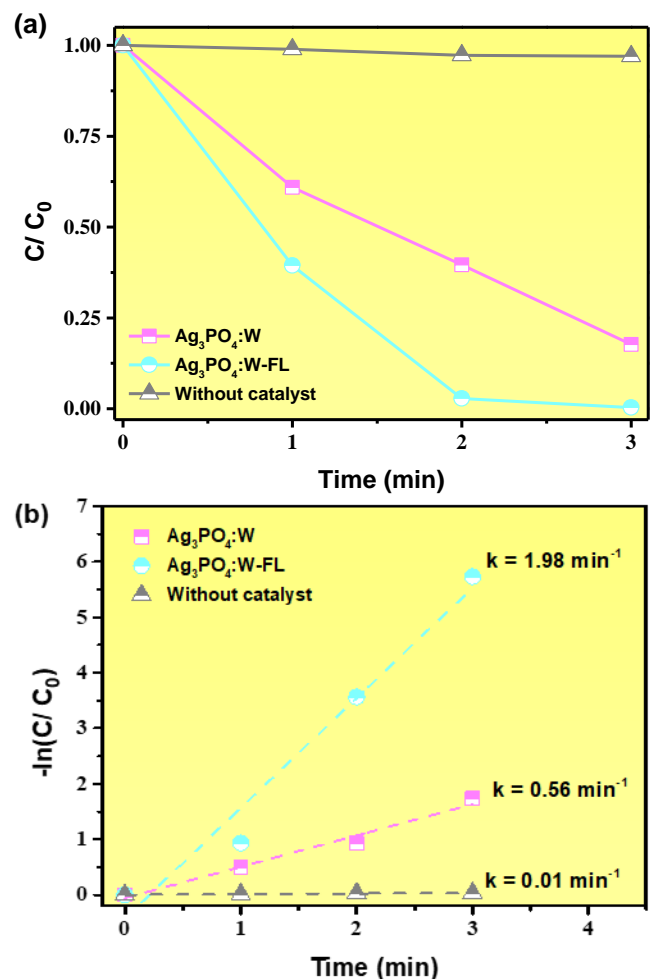


Figure 5. Relative concentration of RhB against reaction time in photocatalytic experiments (a) and pseudo first-order kinetics plot (b) of $\text{Ag}_3\text{PO}_4\text{:W}$ and $\text{Ag}_3\text{PO}_4\text{:W-FL}$ samples.

It has been demonstrated that the FL irradiation in Ag-containing materials induces the formation of Ag nanoparticles, as observed by XRD results and inferred by FE-SEM analysis. The formation of Ag nanoparticles on the surface of Ag_3PO_4 particles results in a semiconductor/metal interface. This interface has an important role in the photocatalytic performance of the $\text{Ag}_3\text{PO}_4\text{:W-FL}$ sample due to the charge carrier transport (Koyappayil *et al.*, 2020; Nubla and Sandhyarani, 2020; Silva *et al.*, 2019; Sofi and Majid, 2019). The visible light irradiation photoexcites electrons from the valence band to the conduction band. The photoexcited electrons

can participate in reduction reactions with the reaction media, but also recombine with the holes in the valence band. The presence of the Ag nanoparticles on the Ag_3PO_4 surface under visible light irradiation can act as electron traps due to the SPR effect. Thus, the photoexcited electrons in the conduction band of AgPO_4 can be transferred to the Ag nanoparticles. These electrons in the Ag nanoparticles can perform the reduction reactions with the reaction media, whereas the holes in the valence band of Ag_3PO_4 can perform the oxidation reactions. Herewith, the electron transfer from the conduction band of Ag_3PO_4 to Ag nanoparticles decreases the recombination rate of the electron-hole pairs, hence increasing their availability to perform the redox reactions. These reactions can be performed directly with the RhB adsorbed on the particle surface and also indirectly by the formation of radical species.

Moreover, as observed by Raman and UV-Vis results, the FL irradiation in $\text{Ag}_3\text{PO}_4\text{:W}$ induced structural disorder in the $[\text{PO}_4]$ clusters, which generated intermediate energy levels within the band gap. These energy levels can also act as traps for photoexcited electrons in the recombination process, thus decreasing the recombination rate of the electron-hole pairs. Therefore, the FL irradiation in $\text{Ag}_3\text{PO}_4\text{:W}$ sample induced the formation of Ag nanoparticles and intermediate energy levels that can act as electron traps, promoting a significant improvement of the photocatalytic performance of the $\text{Ag}_3\text{PO}_4\text{:W}$.

4. Conclusions

The FL irradiation in $\text{Ag}_3\text{PO}_4\text{:W}$ sample induced the formation of metallic Ag and also structural disorder in $[\text{PO}_4]$ clusters, as observed by XRD and Raman results. The FE-SEM indicated the fragmentation and agglomeration of Ag_3PO_4 particles due to the high local energy of the pulsed laser. Further, it was observed the emergence of nanoparticles in the Ag_3PO_4 surface, which can be assigned to the Ag nanoparticles. The structural disorder in the $[\text{PO}_4]$ clusters induced the formation of intermediate energy levels within band gap, as observed by the decrease in its energy. The FL irradiation promoted a significant improvement of the photocatalytic activity of the $\text{Ag}_3\text{PO}_4\text{:W}$ sample, being 3.54 times higher than the non-irradiated sample. This improvement can be attributed to the SPR effect by the formation of Ag nanoparticles and the intermediate energy levels. Both can act as traps for the photoexcited electrons, which increase the availability of the electron-hole pairs to perform the redox reactions with the reaction medium. Therefore, the FL irradiation has proved to be an effective method for the development of

metal-semiconductor heterostructure and for the enhancement of photocatalytic properties.

Authors' contribution

Conceptualization: Trench, A. B.; Longo, E.

Data curation: Trench, A. B.; Teodoro, V.; Trindade, L. G.; Machado, T. R.

Formal Analysis: Trench, A. B.; Teodoro, V.; Trindade, L. G.; Machado, T. R.

Funding acquisition: Not applicable.

Investigation: Trench, A. B.

Methodology: Trench, A. B.; Longo, E.; Minguez-Veja, G.; Cordoncillo, E.; Doñate-Buendía, C.; Andrés, J.

Project administration: Trench, A. B.; Longo, E.

Resources: Longo, E.

Software: Not applicable.

Supervision: Longo, E.

Validation: Trench, A. B.

Visualization: Trench, A. B.

Writing – original draft: Trench, A. B.; Teodoro, V.; Trindade, L. G.; Machado, T. R.; Longo, E.

Writing – review & editing: Trench, A. B.; Longo, E.; Minguez-Veja, G.; Cordoncillo, E.; Doñate-Buendía, C.; Andrés, J.

Data availability statement

All data sets were generated or analyzed in the current study.

Funding

Fundação de Amparo à Pesquisa do Estado de São Paulo (FAPESP). Grant No: 2013/07296-2.

Coordenação de Aperfeiçoamento de Pessoal de Nível Superior - Brasil (CAPES). Finance Code: 001.

Conselho Nacional de Desenvolvimento Científico e Tecnológico (CNPq). Grant No: 142035/2017-3.

Universitat Jaume I. Project: UJI-B2019-30; UJI-B2019-37; UJI-B2019-41.

Ministerio de Ciencia, Innovación y Universidades (Spain). Project: PGC2018094417-B-I00.

Ministerio de Ciencia e Innovación. PID2019-110927RB-I00.

Generalitat Valenciana. PROMETEO/2020/029.

Acknowledgments

The authors are very grateful to the “Serveis Centrals d’Instrumentación Científica” (SCIC) of the University Jaume I for the use of the femtosecond laser.

References

Aljerf, L. High-efficiency extraction of bromocresol purple dye and heavy metals as chromium from industrial effluent by adsorption onto a modified surface of zeolite: Kinetics and equilibrium study. *J. Environ. Manage.* **2018**, *225*, 120–132. <https://doi.org/10.1016/j.jenvman.2018.07.048>

Assis, M.; Cordoncillo, E.; Torres-Mendieta, R.; Beltran-Mir, H.; Mínguez-Vega, G.; Oliveira, R.; Leite, E. R.; Foggi, C. C.; Vergani, C. E.; Longo, E.; Andres, J. Towards the scale-up of the formation of nanoparticles on alpha-Ag₂WO₄ with bactericidal properties by femtosecond laser irradiation. *Sci. Rep.* **2018**, *8* (1), 1884. <https://doi.org/10.1038/s41598-018-19270-9>

Assis, M.; Robeldo, T.; Foggi, C. C.; Kubo, A. M.; Mínguez-Vega, G.; Condoncillo, E.; Beltran-Mir, H.; Torres-Mendieta, R.; Andres, J.; Oliva, M.; Vergani, C. E.; Barbugli, P. A.; Camargo, E. R.; Borra, R. C.; Longo, E. Ag Nanoparticles/alpha-Ag₂WO₄ Composite Formed by Electron Beam and Femtosecond Irradiation as Potent Antifungal and Antitumor Agents. *Sci. Rep.* **2019**, *9*, 9927. <https://doi.org/10.1038/s41598-019-46159-y>

Botelho, G.; Sczancoski, J. C.; Andres, J.; Gracia, L.; Longo, E. Experimental and Theoretical Study on the Structure, Optical Properties, and Growth of Metallic Silver Nanostructures in Ag₃PO₄. *J. Phys. Chem. C* **2015**, *119* (11), 6293–6306. <https://doi.org/10.1021/jp512111v>

Botelho, G.; Andres, J.; Gracia, L.; Matos, L. S.; Longo, E. Photoluminescence and Photocatalytic Properties of Ag₃PO₄ Microcrystals: An Experimental and Theoretical Investigation. *ChemPlusChem* **2016**, *81* (2), 202–212. <https://doi.org/10.1002/cplu.201500485>

Chen, X.; Dai, Y.; Wang, X. Methods and mechanism for improvement of photocatalytic activity and stability of Ag₃PO₄: A review. *J. Alloys Compound* **2015**, *649*, 910–932. <https://doi.org/10.1016/j.jallcom.2015.07.174>

Dong, W.; Lee, C. W.; Lu, X.; Sun, Y.; Hua, W.; Zhuang, G.; Zhang, S.; Chen, J.; Hou, H.; Zhao, D. Synchronous role of coupled adsorption and photocatalytic oxidation on ordered mesoporous anatase TiO₂-SiO₂ nanocomposites generating excellent degradation activity of RhB dye. *Appl. Catal. B* **2010**, *95* (3-4), 197–207. <https://doi.org/10.1016/j.apcatb.2009.12.025>

Fujishima, A.; Honda, K. Electrochemical photolysis of water at a semiconductor electrode. *Nature* **1972**, *238*, 37–38. <https://doi.org/10.1038/238037a0>

He, G.; Yang, W.; Zheng, W.; Gong, L.; Wang, X.; An, Y.; Tian, M. Facile controlled synthesis of Ag₃PO₄ with various morphologies for enhanced photocatalytic oxygen evolution from water splitting. *RSC Advances* **2019**, *9* (32), 18222–18231. <https://doi.org/10.1039/C9RA01306G>

Jette, E. R.; Foote, F. Precision Determination of Lattice Constants. *J. Chem. Phys.* **1935**, *3* (10), 605–616. <https://doi.org/10.1063/1.1749562>

Karimi-Maleh, H.; Kumar, B. G.; Rajendran, S.; Qin, J.; Vadivel, S.; Durgalakshmi, D.; Gracia, F.; Soto-Moscoso, M.; Orooji, Y.; Karimi, F. Tuning of metal oxides photocatalytic performance using Ag nanoparticles integration. *J. Mol. Liq.* **2020**, *314*, 113588. <https://doi.org/10.1016/j.molliq.2020.113588>

Kochuveedu, S. T.; Jang, Y. H.; Kim, D. H. A study on the mechanism for the interaction of light with noble metal-metal oxide semiconductor nanostructures for various photophysical applications. *Chem. Soc. Rev.* **2013**, *42* (21), 8467–8493. <https://doi.org/10.1039/c3cs60043b>

Koyappayil, A.; Berchmans, S.; Lee, M.-H. Dual enzyme-like properties of silver nanoparticles decorated Ag₂WO₄ nanorods and its application for H₂O₂ and glucose sensing. *Colloids Surf. B Biointerfaces* **2020**, *189*, 110840. <https://doi.org/10.1016/j.colsurfb.2020.110840>

Lemos, P. S.; Silva, G. S.; Roca, R. A.; Assis, M.; Torres-Mendieta, R.; Beltrán-Mir, H.; Mínguez-Vega, G.; Andrés, J.; and Longo, E. Laser and electron beam-induced formation of Ag/Cr structures on Ag₂CrO₄. *Phys. Chem. Chem. Phys.* **2019**, *21* (11), 6101–6111. <https://doi.org/10.1039/c8cp07263a>

Li, X.; Xu, P.; Chen, M.; Zeng, G.; Wang, D.; Chen, F.; Tang, W.; Chen, C.; Zhang, C.; Tan, X. Application of silver phosphate-based photocatalysts: Barriers and solutions. *Chem. Eng. J.* **2019**, *366*, 339–357. <https://doi.org/10.1016/j.cej.2019.02.083>

Liu, Y.; Fang, L.; Lu, H.; Liu, L.; Wang, H.; Hu, C. Highly efficient and stable Ag/Ag₃PO₄ plasmonic photocatalyst in visible light. *Catal. Commun.* **2012**, *17*, 200–204. <https://doi.org/10.1016/j.catcom.2011.11.001>

Liu, B.; Zhao, X.; Terashima, C.; Fujishima, A.; Nakata, K. Thermodynamic and kinetic analysis of heterogeneous photocatalysis for semiconductor systems. *Phys. Chem. Chem. Phys.* **2014**, *16* (19), 8751–8760. <https://doi.org/10.1039/c3cp55317e>

Liu, Z.; Liu, Y.; Xu, P.; Ma, Z.; Wang, J.; Yuan, H. Rational Design of Wide Spectral-Responsive Heterostructures of Au Nanorod Coupled Ag₃PO₄ with Enhanced Photocatalytic Performance. *ACS Appl. Mater. Interfaces* **2017**, *9* (24), 20620–20629.

- Machado, T. R.; Macedo, N. G.; Assis, M.; Doñate-Buendia, C.; Mínguez-Vega, G.; Teixeira, M. M.; Foggi, C. C.; Vergani, C. E.; Beltran-Mir, H.; Andres, J.; Cordoncillo, E.; Longo, E. From Complex Inorganic Oxides to Ag-Bi Nanoalloy: Synthesis by Femtosecond Laser Irradiation. *ACS omega* **2018**, *3* (8), 9880–9887. <https://doi.org/10.1021/acsomega.8b01264>
- Masse, R.; Torjman, I.; Durif, A. Refinement of Crystal-Structure of Silver Monophosphate, Ag_3PO_4 -Existence of High-Temperature Form. *Zeitschrift Fur Kristallographie* **1976**, *144*, 76–81. <https://doi.org/10.1524/zkri.1976.144.1-6.76>
- Nubla, K.; Sandhyarani, N. Ag nanoparticles anchored Ag_2WO_4 nanorods: An efficient methanol tolerant and durable Pt free electro-catalyst toward oxygen reduction reaction. *Electrochim. Acta* **2020**, *340*, 135942. <https://doi.org/10.1016/j.electacta.2020.135942>
- Santos, C. C.; Assis, M.; Machado, T. R.; Pereira, P. F. S.; Mínguez-Vega, G.; Cordoncillo, E.; Beltran-Mir, H.; Doñate-Buendía, C.; Andrés, J.; Longo, E. Proof-of-concept studies directed toward the formation of metallic Ag nanostructures from Ag_3PO_4 induced by electron beam and femtosecond laser. *Part. Part. Syst. Charact.* **2019**, *36* (6), 1800533. <https://doi.org/10.1002/ppsc.201800533>
- Santos, R. K.; Martins, T. A.; Silva, G. N.; Conceição, M. V. S.; Nogueira, I. C.; Longo, E.; Botelho, G. $\text{Ag}_3\text{PO}_4/\text{NiO}$ Composites with Enhanced Photocatalytic Activity under Visible Light. *ACS omega* **2020**, *5* (34), 21651–21661. <https://doi.org/10.1021/acsomega.0c02456>
- Shaveisi, Y.; Sharifnia, S. Deriving $\text{Ag}_3\text{PO}_4/\text{CaO}$ composite as a stable and solar light photocatalyst for efficient ammonia degradation from wastewater. *J. Energy Chem.* **2018**, *27* (1), 290–299. <https://doi.org/10.1016/j.jechem.2017.06.012>
- Shi, H.; Yang, S.; Han, C.; Niu, Z.; Li, H.; Huang, X.; Ma, J. Fabrication of $\text{Ag}/\text{Ag}_3\text{PO}_4/\text{WO}_3$ ternary nanoparticles as superior photocatalyst for phenol degradation under visible light irradiation. *Solid State Sci.* **2019**, *96*, 105967. <https://doi.org/10.1016/j.solidstatesciences.2019.105967>
- Silva, E. Z.; Faccin, G. M.; Machado, T. R.; Macedo, N. G.; Assis, M.; Maya-Johnson, S.; Sczancoski, J. C.; Andrés, J.; Longo, E.; San-Miguel, M. A. Connecting Theory with Experiment to Understand the Sintering Processes of Ag Nanoparticles. *J. Phys. Chem. C* **2019**, *123* (17), 11310–11318. <https://doi.org/10.1021/acs.jpcc.9b02107>
- Sofi, F. A.; Majid, K. Plasmon induced interfacial charge transfer across Zr-based metal-organic framework coupled Ag_2WO_4 heterojunction functionalized by Ag NPs: Efficient visible light photocatalyst. *Chem. Phys. Lett.* **2019**, *720*, 7–14. <https://doi.org/10.1016/j.cplett.2019.02.005>
- Sousa, J. C. G.; Ribeiro, A. R.; Barbosa, M. O.; Pereira, M. F. R.; Silva, A. M. T. A review on environmental monitoring of water organic pollutants identified by EU guidelines. *J. Hazard. Mater.* **2018**, *344*, 146–162. <https://doi.org/10.1016/j.jhazmat.2017.09.058>
- Tan, D.; Zhou, S.; Qiu, J.; Khusro, N. Preparation of functional nanomaterials with femtosecond laser ablation in solution. *J. Photochem. Photobiol. C Photochem. Rev.* **2013**, *17*, 50–68. <https://doi.org/10.1016/j.jphotochemrev.2013.08.002>
- Trench, A. B.; Machado, T. R.; Gouveia, A. F.; Assis, M.; Trindade, L. G.; Santos, C.; Perrin, A.; Perrin, C.; Oliva, M.; Andrés, J.; Longo, E. Connecting structural, optical, and electronic properties and photocatalytic activity of $\text{Ag}_3\text{PO}_4:\text{Mo}$ complemented by DFT calculations. *Appl. Catal. B* **2018**, *238*, 198–211. <https://doi.org/10.1016/j.apcatb.2018.07.019>
- Trench, A. B.; Machado, T. R.; Gouveia, A. F.; Foggi, C. C.; Teodoro, V.; Sánchez-Montes, I.; Teixeira, M. M.; Trindade, L. G.; Jacomaci, N.; Perrin, A.; Perrin, C.; Aquino, J. M.; Andrés, J.; Longo, E. Rational Design of W-Doped Ag_3PO_4 as an Efficient Antibacterial Agent and Photocatalyst for Organic Pollutant Degradation. *ACS omega* **2020**, *5* (37), 23808–23821. <https://doi.org/10.1021/acsomega.0c03019>
- Vorobyev, A. Y.; Guo, C. Direct femtosecond laser surface nano/microstructuring and its applications. *Laser Photonics Rev.* **2013**, *7* (3), 385–407. <https://doi.org/10.1002/lpor.201200017>
- Wood, D. L.; Tauc, J. Weak Absorption Tails in Amorphous Semiconductors. *Phys. Rev. B* **1972**, *5* (8), 3144–3151. <https://doi.org/10.1103/PhysRevB.5.3144>
- Yan, T.; Zhang, H.; Liu, Y.; Guan, W.; Long, J.; Li, W.; You, J. Fabrication of robust $\text{M}/\text{Ag}_3\text{PO}_4$ ($\text{M} = \text{Pt}, \text{Pd}, \text{Au}$) Schottky-type heterostructures for improved visible-light photocatalysis. *RSC Adv.* **2014**, *4* (70), 37220. <https://doi.org/10.1039/C4RA06254J>
- Zangeneh, H.; Zinatizadeh, A. A. L.; Habibi, M.; Akia, M.; Isa, M. H. Photocatalytic oxidation of organic dyes and pollutants in wastewater using different modified titanium dioxides: A comparative review. *J. Ind. Eng. Chem.* **2015**, *26*, 1–36. <https://doi.org/10.1016/j.jiec.2014.10.043>
- Zwara, J.; Grabowska, E.; Klimczuk, T.; Lisowski, W.; Zaleska-Medynska, A. Shape-dependent enhanced photocatalytic effect under visible light of Ag_3PO_4 particles. *J. Photochem. Photobiol. A Chem.* **2018**, *367*, 240–252. <https://doi.org/10.1016/j.jphotochem.2018.08.006>